

CALIBRATION OF [O IV] 26 μm AS A MEASURE OF INTRINSIC AGN LUMINOSITY

J. R. RIGBY^{1,2}, A. M. DIAMOND-STANIC³, & G. ANIANO⁴

ApJ in press; accepted 17 May 2009

ABSTRACT

We compare [O IV] 25.89 μm emission line luminosities with very hard (10–200 keV) X-rays from Swift, Integral, and BeppoSAX for a complete sample of 89 Seyferts from the Revised Shapley–Ames sample. Using Seyfert 1s, we calibrate [O IV] as a measure of AGN intrinsic luminosity, for particular use in high-obscuration environments. With this calibration, we measure the average decrement in 14–195 keV X-ray to [O IV] luminosity ratio for Seyfert 2s compared to type 1s. We find a decrement of 3.1 ± 0.8 for Seyfert 2s, and a decrement of 5.0 ± 2.7 for known Compton-thick Seyfert 2s. These decrements imply column densities of approximately $\log N_H = 24.6 \text{ cm}^{-2}$ and 24.7 cm^{-2} , respectively. Thus, we infer that the average Seyfert 2 is more highly obscured and intrinsically more luminous than would be inferred even from the very hard X-rays. We demonstrate two applications of the hard X-ray to [O IV] ratio. We measure a column density for the extremely obscured NGC 1068 of $\log N_H = 25.3\text{--}25.4 \text{ cm}^{-2}$. Finally, by comparing [O IV] luminosities to total infrared luminosities for twelve bright ultraluminous infrared galaxies, we find that four have substantial AGN contributions.

Subject headings: galaxies: active — galaxies: nuclei — galaxies: Seyfert — infrared: galaxies

1. INTRODUCTION

The optical line [O III] 5007 \AA is widely used to measure the intrinsic luminosity of active galactic nuclei (AGN) (Heckman et al. 2005). However, there are cases, such as Seyfert 2s, ultra-luminous infrared galaxies, and Compton-thick AGN, where the extinction along our line of sight to the narrow line regions may be high, and a more extinction-robust diagnostic may be needed. Meléndez et al. (2008) recently demonstrated a correlation in AGN between the [O IV] 25.89 μm emission line luminosity and the very hard X-ray luminosity (14–195 keV) as measured by the BAT instrument on Swift. The sample of 40 AGN in Melendez et al., selected by hard X-ray-flux, was sufficient to demonstrate a correlation, but insufficient to calibrate the relationship. In a companion paper to this one (Diamond-Stanic et al. 2009), we find that Seyfert 1s and Seyfert 2s from a complete sample have statistically indistinguishable [O IV] luminosity distributions, which further supports [O IV] as an AGN luminosity diagnostic. Here we compare the [O IV] and hard ($E > 10 \text{ keV}$) X-ray luminosities of a complete sample of 89 Seyferts, bolometrically correct the hard X-rays to infer intrinsic AGN luminosities, and calibrate [O IV] as a measure of intrinsic AGN luminosity.

One potential problem with [O IV] 26 μm is that its critical density of $\log n_{crit} = 4.06 \text{ cm}^{-2}$ is lower than, for example, that of [Ne V] 14.32 μm ($\log n_{crit} = 4.70 \text{ cm}^{-2}$), [Ne V] 24.31 μm ($\log n_{crit} = 4.44 \text{ cm}^{-2}$), or [O III] 5007 \AA ($\log n_{crit} = 5.8 \text{ cm}^{-2}$)⁵. Aniano et al. (in prep.) find, using the same Seyfert sample as this paper, that the [Ne V] 14 / [Ne V] 24 μm line ratio is almost always

< 2.0 , which for temperatures of $\leq 3 \times 10^4 \text{ K}$ implies densities below 10^4 cm^{-3} . Thus, [Ne V]/[Ne V] indicates that the densities are below the [O IV] 26 μm critical density, though this measurement applies only to the [Ne V]-emitting portion of the narrow-line region.

Another potential problem, which affects any intrinsic luminosity diagnostic based on emission lines from the narrow-line region (NLR), is that one must assume that the NLR enjoys an unobscured line of sight down to the central engine. If this assumption is violated, then the NLR will be ionized by less than the true continuum strength, and consequently NLR diagnostics will underestimate the intrinsic AGN luminosity.

For now, we develop [O IV] as a luminosity indicator, with the caveats that it may cease to work when densities exceed critical, and that like [O III] 5007 \AA it assumes the narrow line region has not been shielded from the full intensity of the central engine. In §7, we examine [O IV] luminosities in ultra-luminous infrared galaxies (ULIRGs), which as deeply-obscured galaxies may be worst-case environments to test the [O IV] diagnostic.

2. THE SAMPLE AND THE DATA

Calibration of [O IV] against hard X-ray luminosity is best done within a complete sample to avoid flux biases. By contrast, the members of the Melendez et al. sample used to establish the correlation between [O IV] and hard X-ray were selected as bright Swift detections, and therefore may well be biased toward X-ray-brightness. Our sample, which is limited by host galaxy magnitude, is the set of 89 Seyferts from Maiolino & Rieke (1995) and Ho et al. (1997) with $B_T \leq 13$. This Revised Shapley–Ames (RSA, Shapley & Ames 1932) Seyfert sample is described in more detail by Diamond-Stanic et al. (2009). We take distances and classifications from Diamond-Stanic et al. (2009); the median distance is 22 Mpc. Optical spectral classifications of Seyfert 1–1.5 we group as “Seyfert 1”, and we group Seyfert 1.8–2 classifications as “Seyfert 2”.

Electronic address: jrigby@ociw.edu

¹ Observatories, Carnegie Institution of Washington

² Spitzer Fellow

³ Steward Observatory, University of Arizona

⁴ Department of Astrophysical Sciences, Princeton University

⁵ [O IV] and [Ne V] critical densities were calculated at $T = 10^4 \text{ K}$ by Cloudy, v08.00, last described by (Ferland et al. 1998). The [O III] critical density at $T = 10^4 \text{ K}$ is from Osterbrock (1989).

From column densities reported in the literature from X-ray measurements, we classify the AGN into reported Compton–thin, reported Compton–thick, and Seyferts whose column densities are not reported in the literature.

Spectra were obtained by the Infrared Spectrograph (IRS) onboard Spitzer. We use [O IV] fluxes from the LL1 order, as measured and tabulated by Diamond-Stanic et al. (2009). These fluxes have been corrected for contamination from the [Fe II] 25.99 μm emission line, as described by Diamond-Stanic et al. (2009). For the few AGN with undetected [O IV], we use the 3σ upper limit. For the very bright sources NGC 1068 and Circinus, we take ISO/SWS fluxes from Sturm et al. (2002), and for NGC 4945 from Spoon et al. (2000).

We take hard X-ray fluxes from published catalogs:

- Swift BAT (14–195 keV) fluxes from the 22 month survey (Tueller et al. 2009);
- BeppoSAX PDS (20–100 keV) fluxes from Dadina (2007); and
- Integral IBIS (17–60 keV) fluxes from Krivonos et al. (2007).

By using all three hard X-ray satellites, we obtain meaningful upper limits (since the Swift survey was all-sky), probe to fluxes fainter than the Swift all-sky detection limit, and gauge the importance of X-ray variability. Since Integral and BeppoSAX observations were targeted, the depth of coverage is highly non–uniform across the sky, so we do not estimate upper limits on non-detections. Since the Swift/BAT survey by design has fairly uniform all-sky coverage, for non-detections we plot upper limits of $3.1 \times 10^{-11} \text{ erg s}^{-1} \text{ cm}^{-2}$, which is the 4.8σ depth the 22 month Swift survey reached for 90% of the sky (Tueller et al. 2009).

We scale BeppoSAX fluxes to equivalent Swift fluxes using the bolometric corrections calculated in §3 for the Marconi et al. (2004) template; for AGN detected by both instruments the scaled fluxes agree within errors. We scale Integral fluxes by an empirical factor of $\times 1.61$, rather than the factor of $\times 1.99$ derived from the Marconi template. This empirical factor is the best–fit linear relation for RSA Seyferts detected by both Integral and Swift.⁶ The offset from the predicted relation is not surprising, since the Integral fluxes assume the spectral shape of the Crab nebula, which is softer than AGN over this spectral range (the Crab nebula has $\Gamma = 2.14$ over the 1–700 keV range according to Kuiper et al. 2001.)

3. THE BOLOMETRIC CORRECTION

One wants to consider the total amount of “direct” or “intrinsic” AGN emission, which is radiated primarily in the X-ray, UV, and optical. This is the luminosity inferred to have been emitted into 4π steradians before any obscuration. One should separately consider emission that has been absorbed and re-radiated into the infrared, since this will depend on the geometry of the absorbing material. A so-called bolometric correction, based on model spectral energy distributions, is used to translate a luminosity measured at a particular band (for

example, hard X-rays) into the intrinsic luminosity of the AGN. (This is termed a “bolometric correction” in the literature, even when, as in this case, the reprocessed infrared emission is deliberately ignored.) Marconi et al. (2004) constructed a template spectrum using broken power laws in the optical–UV, a Rayleigh–Jeans black-body tail in the near-IR, and a power-law spectrum with $\Gamma = 1.9$ plus a reflection component in the X-ray. The X-ray luminosity was scaled to match the luminosity dependence of α_{OX} measured by Vignali et al. (2003). The resulting templates have lower X-ray–to–intrinsic luminosity ratios than Elvis et al. (1994), as expected since the Elvis et al. (1994) sample was chosen to be X-ray bright. In correcting for that bias, Elvis et al. (2002) shifted the X-ray portion of their template down 0.135 dex; this accounts for all but 0.05 dex of the offset between the Elvis et al. (1994) and Marconi et al. (2004) templates.

From these templates, Marconi et al. calculate the conversion from $L(2–10 \text{ keV})$ to $L(\text{intrinsic})$ as a function of $L(\text{intrinsic})$, and plot the relation in their figure 3b. We simply scale this conversion to higher X-ray energies. Fitting a fifth-order polynomial to the Marconi et al. template and integrating over the relevant X-ray bands, the scaling relations are:

$$f(14 - 195 \text{ keV})/f(2 - 10 \text{ keV}) = 2.67 \quad (1)$$

$$f(20 - 100 \text{ keV})/f(2 - 10 \text{ keV}) = 1.74 \quad (2)$$

$$f(17 - 60 \text{ keV})/f(2 - 10 \text{ keV}) = 1.34 \quad (3)$$

for the Swift BAT, BeppoSAX PDS, and Integral IBIS bands, respectively. We then fit the dependence of intrinsic luminosity L_I on 2–10 keV luminosity L_{2-10} in the Marconi models as:

$$\log(L_I/L_\odot) = 0.03776 [\log(L_{2-10}/L_\odot)]^2 + 0.5340 \log(L_{2-10}/L_\odot) + 2.276 \quad (4)$$

This equation, along with the scaling relations in eqn. 1–3, can be used to infer an intrinsic AGN luminosity from a measured high-energy X-ray luminosity.

The Marconi et al. (2004) template is well–suited to this application because it accounts for the known luminosity dependence of α_{OX} (Vignali et al. 2003), and because it extends in energy up to 1 MeV, unlike for example the Elvis et al. (1994) template which stops at 40 keV. We have already shown that the Marconi et al. (2004) template agrees well with the revised Elvis et al. template (2002), and will thus generate similar bolometric corrections. We now check the bolometric correction against Vasudevan & Fabian (2007). We consider the 54 AGN from Vasudevan & Fabian (2007) that have intrinsic AGN luminosities estimated from FUSE. Sixteen are detected in the Tueller et al. (2009) Swift catalog. In Figure 1 we plot the AGN luminosity from Vasudevan & Fabian (2007) against the Swift BAT luminosity. We plot a simple linear fit considering only detections, as well as a non-linear fit that includes BAT upper limits using the Buckley–James regression method (Isobe et al. 1986). Figure 1 shows that the non-linear fit agrees extremely well with the Marconi relation.

4. COMPARING [O IV] AND HARD X-RAY LUMINOSITIES

⁶ After dropping the two weakest detections.

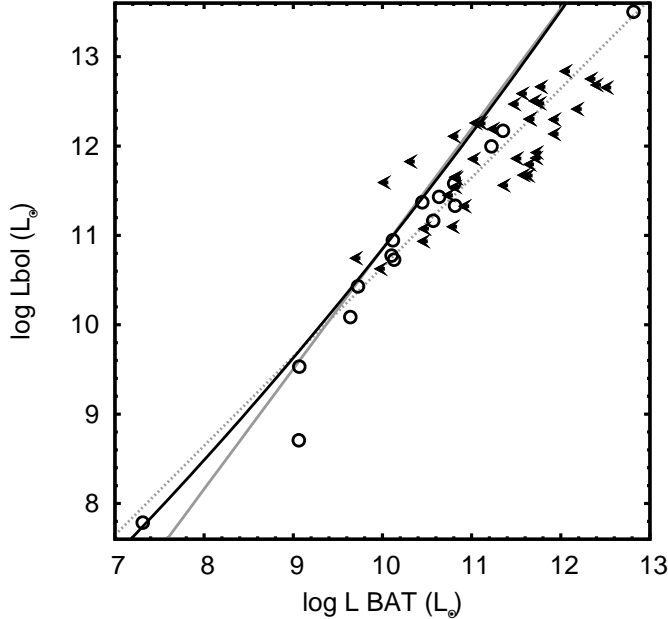


FIG. 1.— Comparison of bolometric luminosity (inferred from FUSE far-UV) and Swift BAT hard X-ray luminosity for the 16 AGN in Vasudevan & Fabian (2007) detected by BAT. Two fits are plotted: a proportional fit to the detections (*dashed line*) of $L_I/L_\odot = 4.42 L_{BAT}$; and a non-linear fit that includes the BAT upper limits using the Buckley-James regression method (*grey solid line*) of $\log(L_I/L_\odot) = 1.345 \log(L_{BAT}/L_\odot) - 2.60$. The non-linear fit agrees extremely well with the relation from Marconi et al. (2004) (*black solid line*), where a bolometric correction has been applied between BAT and 2–10 keV.

Figure 2 plots Swift-equivalent luminosity against [O IV] luminosity. Each detection is plotted separately, with symbols to indicate the satellite (squares for Swift, circles for BeppoSAX, triangles for Integral). (For example, an AGN detected by all three satellites is represented by a cluster of three points at the same $L[\text{O IV}]$ value.) The AGN are split into four panels using classifications described in §2: Seyfert 1; Compton-thin Seyfert 2; Seyfert 2 with unknown column density; and Compton-thick Seyfert 2.

Next, we use the bolometric corrections of Marconi et al. (2004) to convert the Swift-equivalent X-ray luminosities into intrinsic AGN luminosity, and plot against $L[\text{O IV}]$ in Figure 3. Symbols indicate column density and spectral classification. We confirm the result of Meléndez et al. (2008) that Seyfert 2s have systematically lower X-ray/[OIV] luminosity ratios than Seyfert 1s. In addition, with our larger sample of 18 Compton-thick AGN (compared to 4 in Meléndez et al. (2008)), of which 15 were detected in [O IV], and 6 were detected in hard X-ray, we show that Compton-thick AGN have still lower ratios.

For each AGN class, we fit the ratio of intrinsic AGN luminosity inferred from the hard X-rays to [O IV] luminosity using the Kaplan-Meier estimator of the survival function (Feigelson & Nelson 1985), as implemented in the ASURV package (LaValley et al. 1992). This estimator incorporates both detections and upper limits to provide a maximum likelihood reconstruction of the true distribution function, even in cases where there are more upper limits than detections (as for the Compton-thick

AGN.)

For AGN detected by multiple X-ray instruments, we use the average scaled X-ray flux. For Seyfert 1s, the best-fit ratio is 2550 ± 740 (with a scatter of 0.4 dex); for Seyfert 2s it is 810 ± 170 ; for known Compton-thin Seyfert 2s it is 1320 ± 300 ; and for known Compton-thick Seyfert 2s it is 510 ± 270 .⁷ If we exclude the anomalously X-ray-bright NGC 4945 from the fit, the best-fit ratio for the Compton-thick Seyfert 2s falls to 240 ± 70 .⁸ Thus, Seyfert 2s have an average hard X-ray to [O IV] ratio that is 3.1 ± 0.8 times lower than Seyfert 1s. Known Compton-thin Seyfert 2s show a decrement of 1.9 ± 0.5 , and known Compton-thick Seyfert 2s show a decrement of 5.0 ± 2.7 (excluding NGC 1068.)

The two-sample ASURV statistical tests find a $< 0.06\%$ probability that the X/[O IV] ratios for Seyfert 1s and Seyfert 2s are drawn from the same population. It is similarly improbable ($< 0.09\%$) that Seyfert 1s and Compton-thick Seyfert 2s are drawn from the same population. However, the offset between S1s and Compton-thin Seyfert 2s is of lower statistical significance (9% probability of being drawn from the same population).

5. ESTIMATING COLUMN DENSITIES

We now interpret the difference in hard X-ray/[O IV] ratio between type 1 and type 2 Seyferts. One explanation would be that the [O IV] luminosities for the type 1 Seyferts are biased high. In a companion paper (Diamond-Stanic et al. 2009), we find no significant differences between the [O IV] luminosity distributions of type 1 and type 2 Seyferts; the same conclusion can be reached by inspecting Figures 2 and 3. Thus, there is no evidence for a bias toward high [O IV] luminosities.

Therefore, we use $L[\text{O IV}]$ as a measure of intrinsic AGN luminosity, and interpret the offset in hard X-ray/[O IV] ratios as caused by substantial absorption in the $E > 10$ keV spectra of Seyfert 2s, as suggested by Meléndez et al. (2008). At such high energies, the cross-section for Compton scattering is larger than that of photoelectric absorption. Consequently, one expects a typical high-energy photon to experience multiple Compton scatterings, losing energy each time to electron recoil, until the photon either escapes, or loses sufficient energy and traverses a sufficient path that it is absorbed photoelectrically. This makes the problem relativistic, optically-thick, and geometry-dependent, and as such, Monte Carlo simulations are required to interpret the flux decrement. Fortunately, Matt et al. (1999) simulated exactly this situation. We numerically integrate their spectra over the Swift/BAT, BeppoSAX/PDS, and Integral/IBIS energy bands and compare to the injected spectrum; the resulting flux decrements are listed in Table 1.

In the Matt et al. (1999) model, suppressing a BAT flux by a factor of 3.1 ± 0.8 (as observed for all Seyfert 2s in our sample) requires a column density of $\log N(H) = 24.6^{+0.1}_{-0.2} \text{ cm}^{-2}$. Suppression by a factor of 5.0 ± 2.7 (as observed for known Compton-thick Seyfert 2s⁹) requires $\log N(H) = 24.7^{+0.2}_{-0.3} \text{ cm}^{-2}$. These results are consistent

⁷ We exclude NGC 1068 from the fit because its ratio is so low, and consider it separately in §6.

⁸ Excluding NGC 1068 as well.

⁹ Excluding NGC 1068.

with the column density of $\log N(H) = 24.5 \pm 0.1$ inferred by Meléndez et al. (2008) for their sample of 17 Seyfert 2s. Thus, the [O IV] to hard X-ray ratio confirms that, on average, Seyfert 2s are more obscured in the hard X-rays than Seyfert 1s, and predicts the obscuring column densities expected for Compton-thick AGN.

Surprisingly, the average ratio for the known Compton-thin Seyfert 2s also suggests high columns. Suppression by a factor of 1.9 ± 0.5 can be explained by $\log N(H) = 24.3_{-0.3}^{+0.1} \text{ cm}^{-2}$. By contrast, the median column density reported in the literature for these AGN, based on 2–10 keV measurements, is $\log N(H) = 23.0 \text{ cm}^{-2}$ (Diamond-Stanic et al. 2009). As such, the hard X-ray/[O IV] ratios imply higher columns (Compton-thick or nearly so) than inferred from the 2–10 keV spectra. However, this is not the only plausible interpretation. As discussed in §4, the offset in hard X-ray/[O IV] ratio between Compton-thin Seyfert 2s and Seyfert 1s is of low statistical significance in our sample. As such, we cannot rule out Compton-thin Seyfert 2s having, on average, low columns. Table 1 shows that column densities below $\log N(H) \sim 24 \text{ cm}^{-2}$ should produce only a small flux decrement. Accordingly, for such low columns, soft X-ray spectra should return a more precise measurement of the column density.

Figure 3 does show that a substantial minority of the Compton-thin Seyfert 2s have X/[O IV] ratios as low as known Compton-thick AGN. In order of increasing X/[O IV] ratio, these are NGC 1365, NGC 7582, NGC 2992, NGC 7314, NGC 3081, and NGC 5728.¹⁰ There several possible explanations for these low ratios: they may have nearly Compton-thick or Compton-thick columns, have column densities that vary dramatically with time, or have dramatic variations in hard X-ray flux. The literature reveals that all three explanations appear to be at work:

- NGC 1365 varies between Compton-thin and Compton-thick in a matter of days (Risaliti et al. 2007);
- NGC 7582 has experienced dramatic changes in its 2–10 keV flux consistent with a variable Compton-thick absorber (Piconcelli et al. 2007);
- NGC 2992 was measured to have a column of only $7 \times 10^{21} \text{ cm}^{-2}$ (Colbert et al. 2005), but its 2–10 keV flux has varied by a factor of 20 over twenty years (Gilli et al. 2000), and its BAT flux has varied by a factor of 6 (Beckmann et al. 2007);
- NGC 7314 was measured to have a low column density (Risaliti 2002);
- NGC 3081 was measured to have a column density of $6 \times 10^{23} \text{ cm}^{-2}$ (Maiolino et al. 1998), and varies in the BAT band by a factor of 7 (Beckmann et al. 2007);
- NGC 5728 is borderline Compton thick with a column of $8 \times 10^{23} \text{ cm}^{-2}$ (Zhang et al. 2006).

¹⁰ The remaining Compton-thin Seyfert 2s have an average hard X-ray to [O IV] offset from the Seyfert 1s that is of even lower statistical significance.

Thus, five of these six AGN have a plausible explanation for their low X/[O IV] ratios; in four cases the explanation appears to be that the column is almost Compton-thick, or transitions between Compton thick and thin. This comparison also suggests that an inherent drawback of calibrating [O IV] against the hard X-rays is that the hard X-ray flux may vary with time. Still, the systematically low X/[O IV] ratios observed for all Seyfert 2s in this sample strongly suggest that the typical Seyfert 2 has a significantly attenuated hard X-ray flux, and is considerably more powerful than would be inferred from the hard X-rays.

6. APPLICATION: NGC 1068

The famous Compton-thick NGC 1068 is the most highly-obscured AGN in our sample, based on its hard X-ray to [O IV] luminosity ratio. Its [O IV] luminosity¹¹ of $1.2 \times 10^8 L_{\odot}$ predicts an intrinsic AGN luminosity of $(3.1 \pm 0.9) \times 10^{11} L_{\odot}$ using the Seyfert 1 calibration. The [O IV] flux is taken from high resolution ISO spectra (Sturm et al. 2002), so [Fe II] contamination is not an issue; in any case the [Fe II] line strength is only 4% that of [O IV]. The hard X-ray to [O IV] ratio is 490× lower than the Seyfert 1 best fit, implying a column density of $\log N_H = 25.3$ to 25.4 cm^{-2} in the Matt et al. (1999) models. (The column should be still higher if scattered light contributes substantially to the observed X-ray flux.) This inferred column is consistent with the lower limits inferred through a similar comparison to [O III] 5007Å (Matt et al. 1997, 2000). In a future paper, we plan to compare this inferred intrinsic luminosity in detail with the reprocessed mid-infrared SED.

7. APPLICATION: ULTRA-LUMINOUS INFRARED GALAXIES

As an application of the [O IV] calibration, we consider the [O IV] luminosities for twelve nearby ultra-luminous infrared galaxies (ULIRGs), using data from Armus et al. (2004) and Armus et al. (2007), which comprises the ten brightest ULIRGs plus two others. Only five ULIRGs have detected [O IV]: IRAS 05189-2524, IRAS 13428+5608 (Mrk 273), IRAS 09320+6134 (UGC 5101), Mrk 1014, and Mrk 463e. Using the relation established above for Seyfert 1s, we infer intrinsic AGN luminosities from L[O IV] and compare to the total infrared (8–1000 μm) luminosities. The inferred L(AGN)/L(IR) percentages are 49%, 97%, 22%, 170%, and 520%, respectively. (A 30% errorbar should be applied for the uncertainty in the Seyfert 1 calibration.) For ULIRGs with undetected [O IV] we infer percentages below 8%.

Based on excitation diagrams using [Ne V]/[Ne II], [O IV]/[Ne II], and the equivalent width of the 6.2 μm PAH feature, Armus et al. (2007) picked out three of these (Mrk 463e, Mrk 1014, and IRAS 05189-2524) as being likely AGN-dominated. In addition, they estimate Mrk 273 has an AGN contribution of 50–70%. UGC 5101, which [O IV] indicates has a modest AGN contribution, does not stand out as AGN-dominated in the Armus et al. (2007) excitation diagrams; however, it does have detected Fe K α with an equivalent width of 400 eV (Imanishi et al. 2003), which signals that an obscured AGN is present and may possibly be bolometri-

¹¹ Assuming a distance of 14.4 Mpc.

cally important. Thus, the $L[\text{O IV}]/L(\text{IR})$ ratio gives results consistent with the excitation diagrams as to which ULIRGs are AGN-dominated.

Does the normalization of $L[\text{O IV}]$ to $L(\text{AGN})$, calibrated from Seyfert 1s, appear roughly correct for ULIRGs? The preliminary answer appears to be yes, since the inferred AGN fractions are of order unity for four of the five the [O IV]-detected ULIRGs, consistent with the results of the excitation diagrams. Armus et al. (2007) did note that the AGN fractions implied by $[\text{Ne V}]/[\text{Ne II}]$ or $[\text{O IV}]/[\text{Ne II}]$ line ratios were significantly lower than implied by the mid-IR slope or the $6.2 \mu\text{m}$ PAH feature equivalent width; we do not see this effect for $L[\text{O IV}]/L(\text{IR})$. The one clear outlier in $L[\text{O IV}]/L(\text{IR})$ is Mrk 463e, for which we infer an $L(\text{AGN})/L(\text{IR})$ ratio significantly above unity. Such a result is physically plausible if most of the AGN energy is not reprocessed into the infrared, but escapes via the X-ray/UV/optical. Indeed, the infrared luminosity for Mrk 463e is only $5 \times 10^{11} L_{\odot}$, below the ULIRG cutoff, but its total luminosity is considerably higher, well above the ULIRG threshold (Armus et al. 2004). In addition, Mrk 463e has remarkably weak PAH features, which argues that the starburst contribution is small. Thus, given that Mrk 463e is apparently an AGN-dominated ULIRG with a low ratio of reprocessed to intrinsic light, the high measured ratio of $L[\text{O IV}]/L(\text{IR})$ seems reasonable and physical.

It remains unclear how to interpret the [O IV] non-detected ULIRGs, especially those like Mrk 231, which is a broad-line AGN. One explanation is that these galaxies are indeed dominated bolometrically by star formation, not AGN. An alternate explanation would be that they have bolometrically-important AGN, but that the [O IV] diagnostic has failed, perhaps because densities exceed the [O IV] critical density, or because the narrow line regions have been shielded from the central engine. Thus, while the [O IV] diagnostic appears to work well for Seyferts in the RSA sample, and identifies what are thought to be the most AGN-dominated of bright ULIRG, more work is still required to understand its strengths and limitations of the diagnostic in extremely obscured environments.

8. CONCLUSIONS

We present the first calibration of [O IV] $25.89 \mu\text{m}$ as a measure of intrinsic AGN luminosity. The [O IV] line is bright, is detected in hundreds of AGN in the Spitzer archive, and will be detectable to Herschel and JWST.

We find that Seyfert 2s show systematically lower ($E > 10 \text{ keV}$) ratios of X-ray to [O IV] luminosity than Seyfert 1s, by a factor of 3.1 ± 0.8 . For AGN previously identified as Compton-thick, the observed decrement is 5.0 ± 2.7 . We interpret this as caused by absorption that affects even the very hard X-rays. Monte Carlo simulations (Matt et al. 1999) associate these X-ray/[O IV] flux decrements with average column densities of $\log N(H) = 24.6_{-0.2}^{+0.1} \text{ cm}^{-2}$ and $24.7_{-0.3}^{+0.2} \text{ cm}^{-2}$, respectively. This, we find substantial obscuration in most Seyfert 2s.

We briefly explore use of [O IV] $26 \mu\text{m}$ to estimate AGN power even in very obscured systems such as Compton-thick AGN and ULIRGs. For Compton-thick AGN we infer sensible average column densities, and

are able to infer a column density even for the extremely obscured NGC 1068. Application to ULIRGs is less straightforward, since only five of the twelve bright ULIRGs we examine have detected [O IV]. For [O IV]-detected ULIRGs, the $L(\text{O IV})/L(\text{IR})$ ratios imply significant AGN contribution. The question remains whether the non-detections have lower AGN fractions than the detections; it is possible that the [O IV] diagnostic breaks down in the extreme environments of some ULIRGs.

We conclude by noting the recent interest in using very hard X-rays to find obscured AGN, due to their penetrating power. Several sensitive, high-resolution $E > 10 \text{ keV}$ wide-field or pencil-beam X-ray satellites are now in preparation or planning, with scientific goals of finding even the most obscured AGN in the nearby universe, and identifying the population of Compton-thick AGN presumed to contribute to the hardness of the X-ray background. Our results suggest that even the 20–200 keV band suffers considerable flux attenuation in typical Seyfert 2s, especially those that are Compton-thick. Thus, our results predict that X-ray surveys will probe considerably smaller volumes for obscured AGN than for unobscured AGN, even when very hard energy bands are used. The [O IV] $26 \mu\text{m}$ line may play a critical role in measuring this absorption, and determining the true luminosities of even highly-obscured AGN.

Acknowledgments: We thank G. Matt for kindly providing Monte Carlo simulation results from Matt et al. (1999) for additional column densities. JRR was supported by a Spitzer Space Telescope Postdoctoral Fellowship.

TABLE 1
RATIO OF EMERGENT TO INPUT HARD X-RAY FLUX, FROM
MATT ET AL. (1999) MODELS.

$\log N_H$ (cm^{-2})	Swift/BAT	SAX/PDS	Integral/IBIS
23.0	0.96	0.96	0.96
23.5	0.88	0.89	0.87
23.8	0.78	0.80	0.77
24.0	0.69	0.71	0.68
24.1	0.64	0.66	0.63
24.2	0.58	0.61	0.57
24.3	0.51	0.54	0.50
24.4	0.44	0.48	0.44
24.5	0.37	0.41	0.38
24.6	0.30	0.34	0.31
24.7	0.23	0.27	0.25
24.8	0.17	0.20	0.19
24.9	0.11	0.13	0.13
25.0	0.063	0.077	0.074
25.1	0.048	0.058	0.056
25.2	0.028	0.034	0.033
25.3	0.0032	0.0039	0.0039
25.4	0.0016	0.0020	0.0020
25.5	0.00010	0.00013	0.00013

REFERENCES

- Armus, L., et al. 2004, *ApJS*, 154, 178
 Armus, L., et al. 2007, *ApJ*, 656, 148
 Brandl, B. R., et al. 2006, *ApJ*, 653, 1129
 Beckmann, V., Gehrels, N., & Tueller, J. 2007, *ApJ*, 666, 122
 Colbert, E. J. M., Strickland, D. K., Veilleux, S., & Weaver, K. A. 2005, *ApJ*, 628, 113
 Dadina, M. 2007, *A&A*, 461, 1209
 Diamond-Stanic, A. M., Rieke, G. H., & Rigby, J. R. 2009, *ApJ* in press
 Elvis, M., Risaliti, G., & Zamorani, G. 2002, *ApJ*, 565, L75
 Elvis, M., et al. 1994, *ApJS*, 95, 1
 Feigelson, E. D., & Nelson, P. I. 1985, *ApJ*, 293, 192
 Feldmeier, J. J., Ciardullo, R., & Jacoby, G. H. 1997, *ApJ*, 479, 231
 Ferland, G. J., Korista, K. T., Verner, D. A., Ferguson, J. W., Kingdon, J. B., & Verner, E. M. 1998, *PASP*, 110, 761
 Freedman, W. L., et al. 2001, *ApJ*, 553, 47
 Gilli, R., Maiolino, R., Marconi, A., Risaliti, G., Dadina, M., Weaver, K. A., & Colbert, E. J. M. 2000, *A&A*, 355, 485
 Heckman, T. M., Ptak, A., Hornschemeier, A., & Kauffmann, G. 2005, *ApJ*, 634, 161
 Ho, L. C., Filippenko, A. V., & Sargent, W. L. W. 1997, *ApJS*, 112, 315
 Imanishi, M., Terashima, Y., Anabuki, N., & Nakagawa, T. 2003, *ApJ*, 596, L167
 Isobe, T., Feigelson, E. D., & Nelson, P. I. 1986, *ApJ*, 306, 490
 Karachentsev, I. D., et al. 2003, *A&A*, 398, 467
 Kuiper, L., Hermsen, W., Cusumano, G., Diehl, R., Schönfelder, V., Strong, A., Bennett, K., & McConnell, M. L. 2001, *A&A*, 378, 918
 Krivonos, R., Revnivtsev, M., Lutovinov, A., Sazonov, S., Churazov, E., & Sunyaev, R. 2007, *A&A*, 475, 775
 LaValley, Isobe, & Feigelson 1992, *Astronomical Data Analysis Software and Systems I*, 25, 245
 Maiolino, R., & Rieke, G. H. 1995, *ApJ*, 454, 95
 Maiolino, R., Salvati, M., Bassani, L., Dadina, M., della Ceca, R., Matt, G., Risaliti, G., & Zamorani, G. 1998, *A&A*, 338, 781
 Marconi, A., Risaliti, G., Gilli, R., Hunt, L. K., Maiolino, R., & Salvati, M. 2004, *MNRAS*, 351, 169
 Matt, G., et al. 1997, *A&A*, 325, L13
 Matt, G., Pompilio, F., & La Franca, F. 1999, *New Astronomy*, 4, 191
 Matt, G., Fabian, A. C., Guainazzi, M., Iwasawa, K., Bassani, L., & Malaguti, G. 2000, *MNRAS*, 318, 173
 Meléndez, M., et al. 2008, *ApJ*, 682, 94
 Osterbrock, D. E. 1989, *Astrophysics of Gaseous Nebulae and Active Galactic Nuclei* (Sausalito: University Science Books)
 Piconcelli, E., Bianchi, S., Guainazzi, M., Fiore, F., & Chiaberge, M. 2007, *A&A*, 466, 855
 Risaliti, G. 2002, *A&A*, 386, 379
 Risaliti, G., Elvis, M., Fabbiano, G., Baldi, A., Zezas, A., & Salvati, M. 2007, *ApJ*, 659, L111
 Sandage, A., & Tammann, G. A. 1987, *Carnegie Institution of Washington Publication*, Washington: Carnegie Institution, 1987, 2nd ed.,
 Shapley, H., & Ames, A. 1932, *Annals of Harvard College Observatory*, 88, 41
 Spinoglio, L., Malkan, M. A., Rush, B., Carrasco, L., & Recillas-Cruz, E. 1995, *ApJ*, 453, 616
 Spoon, H. W. W., Koornneef, J., Moorwood, A. F. M., Lutz, D., & Tielens, A. G. G. M. 2000, *A&A*, 357, 898
 Sturm, E., Lutz, D., Verma, A., Netzer, H., Sternberg, A., Moorwood, A. F. M., Oliva, E., & Genzel, R. 2002, *A&A*, 393, 821
 Telesco, C. M., Becklin, E. E., Wynn-Williams, C. G., & Harper, D. A. 1984, *ApJ*, 282, 427
 Tueller, J., et al. 2009, arXiv:0903.3037
 Vasudevan, R. V., & Fabian, A. C. 2007, *MNRAS*, 381, 1235
 Vignali, C., Brandt, W. N., & Schneider, D. P. 2003, *AJ*, 125, 433
 Zhang, J. S., Henkel, C., Kadler, M., Greenhill, L. J., Nagar, N., Wilson, A. S., & Braatz, J. A. 2006, *A&A*, 450, 933

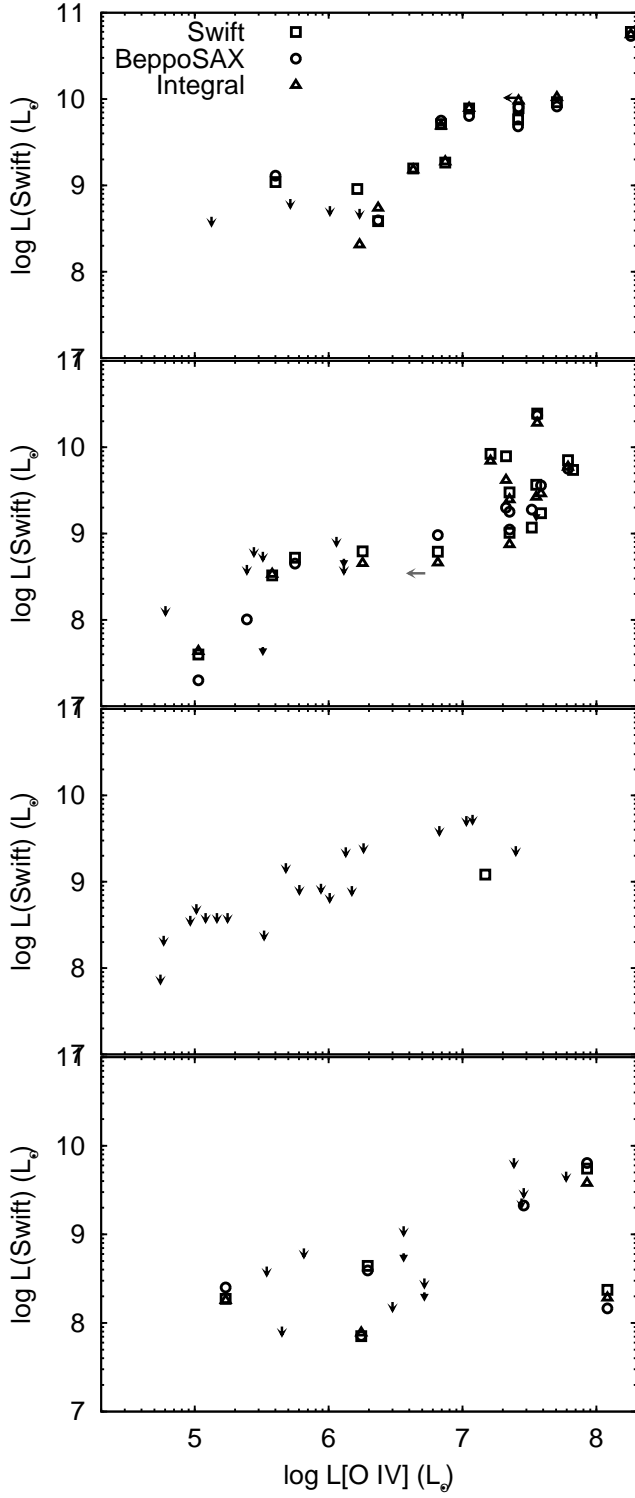


FIG. 2.— Hard X-ray luminosities as a function of [O IV] line luminosity. Seyfert 1 AGN are plotted in the top panel; known Compton-thin Seyfert 2 in the second panel; Seyfert 2 of unknown column density in the third panel; and Compton-thick Seyfert 2 in the bottom panel. Swift BAT detections are squares (upper limits are black partially-filled arrows); BeppoSAX PDS detections are circles (upper limits are black filled arrows); and Integral detections are triangles (upper limits are grey arrows.) BeppoSAX and Integral fluxes have been scaled to equivalent fluxes in the Swift BAT bandpass.

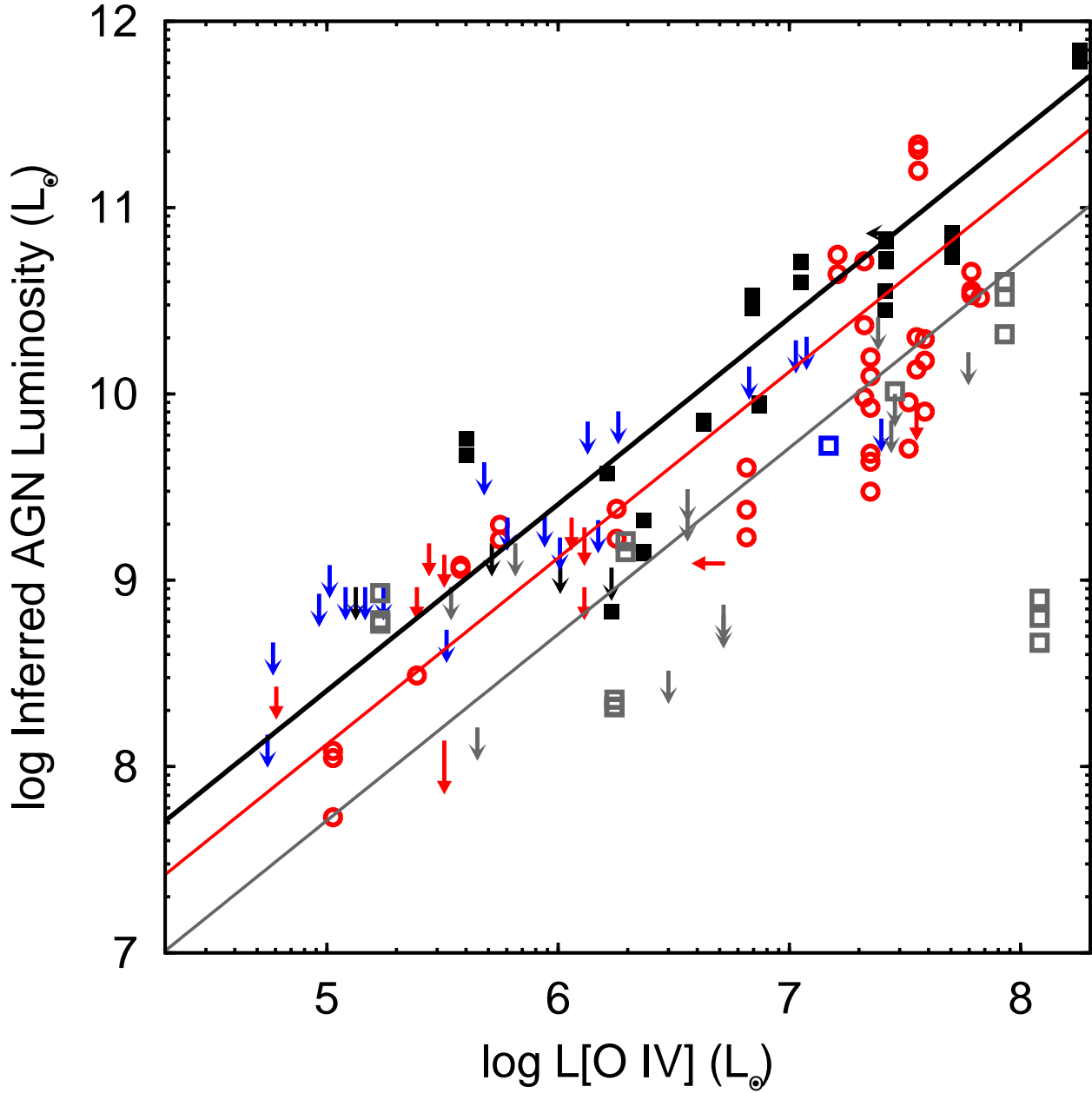


FIG. 3.— Intrinsic AGN luminosity, as inferred from the hard X-rays, versus [O IV] luminosity. Seyfert 1–1.5 AGN are plotted in black as squares (detections) and arrows (non-detections); Compton-thin Seyfert 1.8–2 AGN are plotted as red open circles and arrows; Seyfert 1.8–2 of unknown column are plotted as blue arrows or squares; and Compton-thick AGN are plotted as light grey open squares and arrows. The best fit X-ray–inferred intrinsic to [O IV] luminosity ratio is plotted for each AGN class, in the same color scheme; the fits are given in §4.